Profiling frictional pressure loss in flowing wells: A diagnostic method using conventional pressure-temperature logging

MATSUMOTO, Mitsuo
Department of Earth Resources Engineering, Faculty of Engineering, Kyushu University

KevinYamil GUTIERREZ DONAIRE
Geothermal Studies Division, Nicaraguan Electricity Company

GONNOKAMI, Hiroaki
Exploration & Production Department, Idemitsu Kosan Co., Ltd.

TAKAKI, Keitaro
Department of Earth Resources Engineering, Graduate School of Engineering, Kyushu University

他

https://hdl.handle.net/2324/7173549

出版情報：Journal of the Geothermal Research Society of Japan. 46 (1), pp.21-29, 2024-01-25. THE GEOTHERMAL RESEARCH SOCIETY OF JAPAN

技術報告

Profiling frictional pressure loss in flowing wells: A diagnostic method using conventional pressure–temperature logging

Mitsuo MATSUMOTO*, Kevin Yamil GUTIERREZ DONAIRE**,

Hiroaki GONNOKAMI***, Keitaro TAKAKI****, Kanna SHIGYO****

圧力・温度検層を利用した坑井内摩擦圧力損失の調査手法

松本光央*・ケヴィン ジャミル グティエレス ドナイレ**

・権守宏明***・高木敬太郎****・執行栞夏****

---

* Department of Earth Resources Engineering, Faculty of Engineering, Kyushu University

744 Motooka, Nishi-ku, Fukuoka, 819-0395, Japan

** Geothermal Studies Division, Nicaraguan Electricity Company

Intersección Pista Juan Pablo II y Prologación Avenida Bolívar. Aptdo. 55, Managua, Nicaragua

*** Exploration & Production Department, Idemitsu Kosan Co., Ltd.

1-2-1 Otemachi, Chiyoda-ku, Tokyo, 100-8321, Japan

**** Department of Earth Resources Engineering, Graduate School of Engineering, Kyushu University

744 Motooka, Nishi-ku, Fukuoka, 819-0395, Japan

概要

一般的な圧力・温度検層の既存データ（坑井仕様と流量を含む）を利用した，コスト効率が良い坑井内摩擦圧力損失の調査手法を提案する。本手法では、圧力測定値を坑口圧力・慣性力・摩擦力・重力の各成分に分解して抽出した，摩擦圧力損失のプロファイルを作成する。現実の生産井と試験井に適用した結果，スケール付着，ケーシング径の変化，設置されたマルチステージ・セメンチング用のツールとの対応を示唆するアノマリーと，その時間的変化を見出すことに成功した。更に増角区間終点付近での摩擦圧力損失の増加から，堆積物の存在が推測された。

Abstract

We propose a cost-efficient diagnostic method for profiling frictional pressure loss in a wellbore using the existing data of conventional pressure–temperature logging, along with well specifications and flow rates. Frictional pressure loss is profiled by decomposing the measured pressure into wellhead pressure, inertial, frictional, and gravitational components. Through the application of this method to actual production and testing wells, anomalies associated with scaling, variations in hydraulic diameter, and the presence of a multistage cementing tool were successfully identified, including their temporal variations. The accumulation of solid particles was inferred from the observed increase in frictional pressure loss near the end of the buildup section of well inclination.

Keywords: well, pressure loss, friction, pressure–temperature logging, wellbore flow

1. Introduction

Geothermal power plants have been sustainably operated through numerous efforts to maintain the ground facilities, wells, and reservoirs, as well as social acceptance; all while ensuring profitability. One of the key challenges lies in preventing the irregular halts of production and reinjection wells caused by internal issues. To ensure sustainability, it is crucial to monitor these wells down to their depths, overcoming operational constraints and maintaining cost efficiency. Conventional techniques that monitor parameters at ground level, such as wellhead pressure and production rate, provide limited insights into the wellbore condition. In recent years, state-of-the-art techniques, such as the internet of things and artificial intelligence, have emerged and proven successful in effectively monitoring subsurface including the wellbore (NEDO, 2022). These advancements are expected to significantly enhance the efficiency of geothermal power generation.

We re-evaluated the effectiveness of conventional pressure–temperature logging in inspecting the condition of a wellbore. Considering the equation of motion in a flowing well, we are able to theoretically decompose the measured pressure into components; one of which represents the contribution of friction. Through applications to actual wells, we have found that the frictional pressure component is highly sensitive to temporal and spatial variations in frictional pressure loss, including those caused by scaling, hydraulic diameter variations, and the presence of a multistage cementing tool. Based on these findings, this report proposes a diagnostic method for profiling frictional pressure loss in a wellbore using conventional pressure–temperature logging. If pressure–temperature logging is performed regularly (e.g., every regular shutdown maintenance), the method allows to inspect wells regularly without additional measurements, which will be significantly advantageous for cost efficiency. This report describes the theoretical background and implementation of the method, along with its application to two actual wells. Finally, we discuss the advantages and limitations of the method to facilitate its successful implementation.

2. Theoretical background and implementation

The decomposition of measured pressure into components, which is the basis of the method proposed in this report, is derived from the equation of motion in a flowing well. Applying the steady-state homogeneous flow model (Watson, 2013, p. 135; Yamamura et al., 2017; Matsumoto et al., 2021) to the two-phase flow, with a mean density ρ and mean flow velocity u, we can establish the equation of motion for the measured pressure P at a drilling depth z in a flowing directional well as follows:

$$\rho u \frac{du}{dz} = -\frac{dP}{dz} - \frac{\lambda}{2D}\rho u|u| + \rho g \cos\theta, \tag{1}$$

where λ, D, g, and θ are the Moody friction factor, wellbore inner diameter, gravitational acceleration, and wellbore inclination, respectively. By integrating Eq. (1) from the wellhead ($z = 0$ and $P = P_{\mathrm{wh}}$) to the depth z, the measured pressure P is theoretically decomposed into four components:

$$P = P_{\mathrm{wh}} + P_{\mathrm{i}} + P_{\mathrm{f}} + P_{\mathrm{g}}, \tag{2}$$

where the components P_i, P_f, and P_g represent the contributions of inertial, frictional, and gravitational forces, respectively, and are defined as follows:

$$P_\mathrm{i} = -\int_0^z \rho u \frac{du}{dz} dz, \tag{3}$$

$$P_\mathrm{f} = -\int_0^z \frac{\lambda}{2D} \rho u |u| dz, \tag{4}$$

$$P_\mathrm{g} = \int_0^z \rho g \cos\theta \, dz. \tag{5}$$

Referring to the known values of pressure, temperature, inner diameter, and inclination at each depth, along with the flow rate and wellhead pressure, the inertial component P_i and gravitational component P_g were determined by numerically integrating Eqs. (3) and (5), respectively. The equation of state IAPWS-IF97 (IAPWS, 2007) was employed to determine the density of compressed water and those of saturated water and steam involved in the mean density ρ (Yamamura et al., 2017; Matsumoto et al., 2021) based on the void fraction obeying Smith's formula (Smith, 1969–70) at each depth. In single-phase flow intervals, the mean density was determined from the pressure and temperature. In two-phase flow intervals, the pressure and mean specific enthalpy of saturated water and steam were selected as the independent variables of the mean density. We assumed that the mean specific enthalpy remained constant above the flash point, as heat loss was assumed negligible. The flash point was manually identified based on the pressure–temperature logging data. If we encounter two-phase flow throughout the wellbore, appropriate assumptions will be necessary for the value of mean specific enthalpy. Finally, we obtained the profile of the frictional component P_f from Eq. (2) using the known components P_wh, P_i, and P_g.

We employed the integrated form of the equation of motion (Eq. (1)) to decompose the measured pressure P into components rather than decomposing the pressure gradient dP/dz as seen in preceding studies (Aunzo et al, 1991, p. 2; Grant and Bixley, 2011, p. 126, 161; Watson, 2013, p. 136). This approach allowed us to work directly with the raw data from pressure–temperature logging, preserving data quality without smoothing or other processing techniques. After the decomposition, the frictional pressure loss dP_{f}/dz was determined by numerically differentiating the frictional component P_{f}, which involved smoothing techniques.

In a single-phase flow interval with a large Reynolds number greater than 4000, the friction factor λ obeys the Colebrook equation (Colebrook, 1939). Assuming the divergence of the Reynolds number to infinity, the equation is simplified as follows (Grant and Bixley, 2011, p. 126):

$$\lambda = \{2\log_{10} 3.7 - 2\log_{10}(\varepsilon/D)\}^{-2}, \tag{6}$$

where ε denotes the roughness of the wellbore inner surface. Thus, the profiles of λ and ε in a flowing well at the instant of pressure–temperature logging could be determined from the known frictional pressure loss dP_{f}/dz and Eqs. (4) and (6).

3. Application 1: Production well in the Momotombo field

3-(1) Conditions

We firstly apply the developed method to the vertical production well MT-4 in the Momotombo geothermal field, Nicaragua, using data provided by the Momotombo Power

Company through personal communication. Pressure–temperature logging was performed twice over a four-year interval while maintaining the production at an approximate flow rate and wellhead pressure of 110 t h^{-1} and 0.6 MPaA, respectively. The logging tool reached down to 775.1 and 600.2 m in the first and second runs, respectively, while the total depth of the well was 1435 m. The inner diameter was totally restricted by 7-inch casing pipes owing to production and tieback liners inserted up to the wellhead (Fig. 1). The slotted interval was below 1240 m. Fig. 1

From the temperature profiles of the first and second runs, the flash point was identified at a depth of 441 and 409 m, respectively. In the second run, valid data were partially missing because the wellhead valve temporarily needed to be throttled to pass down the logging tool through an interval of 381–400 m, which was concluded to be due to scaling immediately above the flash point. The pressure and temperature values in this interval were interpolated using sextic-polynomial regression lines determined from seven measured values below and above the interval (Fig. 2). Supplementary inspection in the following year using the Go-Devil tools, gauges for wellbore inner diameter, identified the reduction of inner diameter; the gauge with a size of 4-3/4 inch reached down to 373 m, while that of 2-3/4 inch reached down to 790 m.

3-(2) Results and discussion Fig. 2

The results of the pressure–temperature logging and the decomposition of the measured pressure into components for each run are summarized in Fig. 3. Within four years between the first and second runs (Runs 1 and 2), the temperature in the single-phase flow interval decreased from 218.6 to 215.3°C approximately, which resulted in the flash point ascending from 441 to 409 m (Fig. 3a). A sharp bend was observed in both the pressure and temperature profiles immediately above the flash point. This feature became more evident in Run 2 and yielded higher pressure values than in Run 1 below approximately 400 m, implying an increase in the pressure loss in the wellbore. The measured pressure was successfully decomposed into the inertial P_i, frictional P_f, and gravitational P_g components (Fig. 3b–c). Following gravity, friction was the second-largest component, except for the wellhead pressure component P_wh, which exhibited a sharp bend immediately above the flash point. The inertial component, smaller than the frictional component by one to two orders of magnitude, was insignificant. Fig. 3

The profiles of the frictional pressure loss dP_f/dz, as well as the friction factor λ and roughness ε, were successfully depicted (Fig. 4). The value of dP_f/dz at each depth was determined from P_f using the central finite difference after smoothing with the moving average method (Fig. 4a):

$$\left[\frac{dP_\mathrm{f}}{dz}\right]_i = \frac{\bar{P}_{\mathrm{f},i+n} - \bar{P}_{\mathrm{f},i-n}}{z_{i+n} - z_{i-n}}, \tag{7}$$

where $[dP_\mathrm{f}/dz]_i$ was the frictional pressure loss at a depth z_i corresponding to the i-th data point, obtained using the averaged frictional component $\bar{P}_\mathrm{f}$ with a window size of $N = 2n + 1$. The moving average at the depth z_i was computed as follows:

$$\bar{P}_{\mathrm{f},i} = \frac{1}{N}\sum_{k=i-n}^{i+n} P_{\mathrm{f},k}. \tag{8}$$

The window size N of the moving average was three data points, which corresponded to a depth interval of approximately nine meters owing to the sampling interval (Fig. 2). The spacing of the finite difference was the same as that of the window size (Eq. (7)). Corresponding to the sharp bend of P_{f}, the profile of dP_{f}/dz exhibited a sharp peak immediately above the flash point. From the correspondence between the depths of this peak and the reduction in inner diameter detected using the logging tools, we can conclude that the scaling induced by the flash of the geothermal fluid potentially yielded the local increase in frictional pressure loss. Fig. 4

A peak at the same depth was also observed in the profile of the friction factor λ (Fig. 4b). The value of λ at the peak was approximately two orders of magnitude larger than those at intervals except the peak. In the interval below 600 m, in which the wellbore could be assumed free from scaling, the range of λ approximately 10^{-2}–10^{-1} was comparable with the range 0.008–0.025 in typical geothermal operating conditions (Grant and Bixley, 2011, p. 126). Using Eq. (6), which is valid for single-phase flow, the profile of roughness ε below the flash point was determined from the friction factor (Fig. 4c). The extremely large values of ε up to 10^2 mm, determined by assuming the inner diameter of 7-inch clean casing pipes, above 600 m were potentially due to the scaling that considerably reduced the inner diameter, as identified using the Go-Devil tools.

4. Application 2: Testing well in the Takigami field

4-(1) Conditions

Next, we demonstrate the application to the testing well K-1 drilled during exploration in the Takigami geothermal field, Japan, using data provided by Idemitsu Oita Geothermal Co., Ltd. through personal communication. Pressure–temperature logging was performed twice over a two-year interval at an approximate production rate and wellhead pressure of 180 t h^{-1} and 0.3 MPaA, respectively. The logging tool reached down to 1946.9 and 1948.2 m in the first and second runs, respectively, while the total depth of the well was 1949 m. The inner diameter was restricted by 13-3/8, 9-5/8, and 7-inch casing pipes without slotted intervals, as well as an 8-1/2-inch open hole (Fig. 5). Fig. 5

Airlift pipes with an outer diameter of 2-7/8 inches for initiating production were placed down to 800.6 and 801.3 m in the first and second runs, respectively. The logging tool passed through the airlift pipes, which potentially degraded the data quality, particularly in the two-phase flow interval. The inclination gradually increased below the kickoff point at 960 m and reached 38°. A multistage cementing tool was installed at approximately 1560 m in the 7-inch cased hole. From the temperature profiles of the first and second runs, the flash point was identified at depths of 689.0 and 681.2 m, respectively, which were above the bottom of the airlift pipes.

4-(2) Results and discussion

The results of the pressure–temperature logging and the decomposition of the measured pressure into components for each run are summarized in Fig. 6. The decomposition was applied to the depth interval above the bottom of the 7-inch cased hole (1908 m) to ensure a uniform mass flow rate. The small differences in the pressure and temperature profiles between the first and second runs (Runs 1 and 2) imply stable conditions with adequate recharge of the geothermal fluid to the reservoir (Fig. 6a). The wavy pressure and temperature profiles above the flash point were measured when the logging tool passed through the airlift pipe, which could not accurately reproduce the profiles along the annulus between the casing and the airlift pipes. Below the flash point, the measurement appeared to conserve data quality down to the bottom of the airlift pipes. The measured pressure was successfully decomposed into the inertial P_i, frictional P_f, and gravitational P_g components (Fig. 6b–c). Owing to the small frictional pressure loss, the gravitational component was predominant throughout the wellbore. The expanded profile of the frictional component exhibited an apparent change in slope, corresponding to stepwise changes in the size of the casing pipes from 13-3/8 to 7 inches in an approximate interval of 780–930 m. A locally large slope was observed at 1560 m, where a multistage cementing tool was installed. The inertial component was smaller than the frictional component by one to two orders of magnitude.

Fig. 6

The profile of the frictional pressure loss dP_f/dz successfully highlights the implications of the frictional pressure component P_f below the flash point (Fig. 7a). In the same manner as in the previous application, dP_f/dz was determined using a combination of the moving average and finite difference methods. The window size of the moving average was 101 data points, corresponding to a depth interval of ten meters owing to the sampling interval. The spacing of the finite difference was the same as that of the window size. The frictional pressure loss dP_f/dz varied, corresponding to the hydraulic diameter, difference between the inner diameter of casing pipes and outer diameter of the airlift pipes, at each depth of the wellbore.

A distinct peak was observed at the depth corresponding to the presence of the multistage cementing tool. Additionally, a slight increase appeared near the end of the buildup section of well inclination at 1790 m as indicated by the inclination profile (Fig. 8a). This slight increase in frictional pressure loss was potentially generated by the bed of particles, such as rock and scale, associated with an inclination of up to 38° (Al-Rubaii et al., 2023). The cable tension profile implies that the logging tool roughly descended in the interval below 1600 m, where the inclination exceeded 20° (Fig. 8b).

Fig. 7

Fig. 8

The profiles of the friction factor λ and roughness ε are shown in Fig. 7b–c. The range of λ approximately 10^{-3}–10^{-2} in the 7-inch cased hole was consistent with the typical geothermal operating conditions (0.008–0.025) (Grant and Bixley, 2011, p. 126). The similarity observed between the profiles of Runs 1 and 2 indicates the satisfactory reproducibility of multiple measurements. In the interval of relatively large hydraulic diameters, the small frictional pressure loss degraded the data quality owing to lower signal-to-noise ratios.

5. Advantages and limitations

As demonstrated above, the diagnostic method proposed in this report has enabled to successfully identify anomalies in frictional pressure loss associated with scaling, variation in hydraulic diameter, and the presence of a multistage cementing tool, including their temporal variations. The high sensitivity and conventional nature of this method will be useful for the sustainable operation of geothermal power plants. By regularly inspecting (e.g., every regular shutdown maintenance) and detecting anomalies, potential problems can be identified before they become evident. Importantly, this method relies solely on conventional pressure–temperature logging data, which is frequently and readily available, and can be applied to both existing operating power plants and prospects being explored and developed. This approach offers significant advantages in terms of cost efficiency.

Several limitations need to be considered when applying this method successfully. The theoretical background, described in Section 2, assumes a uniform mass flow rate throughout the depth interval to determine the distribution of mean flow velocity. However, this may not always be the case, especially when multiple feed zones exist or when the geothermal fluid partially flows through the annulus outside the casing pipes. In such situations, assuming the mean flow velocity, which depends on pressure and temperature as well as the mass flow rate, to be temporally constant can potentially enable to detect temporal variations in anomalies through multiple logging runs. We assume that pure water is produced from a liquid-dominated reservoir with a single flash point in the wellbore. For simplicity, the wellbore flow is currently assumed to be obeying the homogeneous flow model (Watson, 2013, p. 135; Yamamura et al., 2017; Matsumoto et al., 2021), which neglects the slip between liquid and vapor phases. Future studies will consider further general conditions, including pressure–temperature logging while discharging dry steam and injecting water. Sophisticated models for two-phase flow such as the slip and drift-flux models, as Tonkin et al. (2021, 2023a, 2023b) exhaustively reviewed, evaluated, and implemented, will improve the accuracy when decomposing the measured pressure into components. As demonstrated in Section 4, measurements taken inside the airlift pipes can significantly degrade the data quality in the two-phase flow interval. Effective solutions to this problem remain unstudied. Any enhancements or improvements to the method should prioritize the use of conventional and cost-efficient techniques to preserve its original advantages.

6. Conclusions

This study proposes a diagnostic method for profiling frictional pressure loss in a wellbore using conventional pressure–temperature logging. The method involves decomposing the measured pressure into the components of wellhead pressure, inertia, friction, and gravity, as derived from the equation of motion. Determining the inertial and gravitational components and eliminating them, as well as the wellhead pressure, from the measured pressure, we could profile the frictional pressure loss through a straightforward procedure.

The proposed method was applied to two actual wells in the Momotombo and Takigami geothermal fields by successfully decomposing the measured pressure into components. The profile of the frictional pressure loss enabled to successfully identify anomalies associated with scaling, variation in hydraulic diameter, and the presence of a multistage cementing tool, including their temporal variations. The accumulation of solid particles was inferred from the observed increase in frictional pressure loss near the end of the buildup section of well inclination.

This method provides a cost-efficient approach to inspecting frictional pressure loss in a wellbore. Successful applications will require adequate understanding of the limitations associated with certain assumptions, such as having known mass flow rates throughout the depth interval and producing from liquid-dominated reservoirs. The homogeneous flow model is currently assumed for two-phase wellbore flow. The degradation of data quality may be compromised when measuring inside airlift pipes.

Nomenclature

D	Wellbore inner or hydraulic diameter [m]
g	Gravitational acceleration [m s^{-2}]
i	Index of a data point [-]
N	Window size of moving average in number of data points [-]
n	Defined as $N = 2n + 1$.
P	Measured pressure [Pa]
P_{f}	Frictional component [Pa]
$\bar{P}_{\mathrm{f}}$	Averaged frictional component [Pa]
P_{g}	Gravitational component [Pa]
P_{i}	Inertial component [Pa]
P_{wh}	Wellhead pressure [Pa]
u	Mean flow velocity of two-phase flow [m s^{-1}]

z Drilling depth [m]

ε Roughness of wellbore inner surface [m]

θ Wellbore inclination [°]

λ Moody friction factor [-]

ρ Mean density of the mixture of liquid and vapor phases [kg m^{-3}]

Acknowledgement

We thank the Momotombo Power Company, the Nicaraguan Electricity Company, Idemitsu Oita Geothermal Co., Ltd., and Idemitsu Kosan Co., Ltd. for their permission to publish their data and technical support to this study, including helpful comments and discussions. We also thank the reviewers for their constructive and helpful comments to improve the manuscript significantly.

References

Al-Rubaii, M., Al-Shargabi, M. and Al-Shehri, D. (2023) A novel automated model for evaluation of the efficiency of hole cleaning conditions during drilling operations. Applied Sciences, **13**, 6464.

Aunzo, Z.P., Bjornsson, G. and Bodvarsson, G.S. (1991) Wellbore models GWELL, GWNACL, and HOLA User's Guide. Lawrence Berkeley Laboratory Report LBL-31428. University of California, Berkeley, 102p.

Colebrook, C.F. (1939) Turbulent flow in pipes, with particular reference to the transition region between the smooth and rough pipe laws. Journal of the Institution of Civil Engineers, **11**, 133–156.

Grant, M.A. and Bixley, P.F. (2011) Geothermal reservoir engineering, second ed. Academic Press, 359p.

International Association for the Properties of Water and Steam (IAPWS) (2007) Revised release on the IAPWS industrial formulation 1997 for the thermodynamic properties of water and steam. IAPWS, 49p.

Matsumoto, M., Itoi, R. and Fujimitsu, Y. (2021) Theoretical study of conditions for generation of periodic wellbore flow due to inflow of a lower-enthalpy fluid. Geothermics, **89**, 101948.

New Energy and Industrial Technology Development Organization (NEDO) (2022) R&D for Innovative Technologies Applied to Geothermal Exploration and Exploitation. NEDO website, https://www.nedo.go.jp/english/activities/activities_ZZJP_100198.html, accessed June 10, 2023.

Smith, S.L. (1969–70) Void fractions in two-phase flow: A correlation based upon an equal velocity head model. Proceedings of Thermodynamics and Fluid Mechanics Group, **184**, Part 1, 36, 647–664.

Tonkin, R.A., O’Sullivan, M.J. and O’Sullivan, J.P. (2021) A review of mathematical models for geothermal wellbore simulation. Geothermics, **97**, 102255.

Tonkin, R., O'Sullivan, J., Gravatt, M. and O'Sullivan, M. (2023a) Simulation of complex transient flows in geothermal wells. Geothermics, **108**, 102631.

Tonkin, R., O'Sullivan, J., Gravatt, M. and O'Sullivan, M. (2023b) A transient geothermal wellbore simulator. Geothermics, **110**, 102653.

Watson, A. (2013) Geothermal engineering: Fundamentals and applications. Springer, 336p.

Yamamura, K., Itoi, R., Tanaka, T. and Iwasaki, T. (2017) Numerical analysis of transient steam-water two-phase flow in geothermal production wells with multiple feed zones. Proceedings of the 42nd Workshop on Geothermal Reservoir Engineering, Stanford University, Stanford, California, SGP-TR-212.

List of tables and figures

Figures

Fig. 1 Assumed casing hydraulic diameter for decomposing the measured pressure at the production well MT-4 along with the schematic casing program.

Fig. 2 Interpolating missing pressure and temperature values for the second run (Run 2) of the pressure–temperature logging at the production well MT-4.

Fig. 3 (a) Results of the pressure–temperature logging for the first and second runs (Runs 1 and 2) at the production well MT-4. (b, c) Decomposition of the measured pressure into components for each run.

Fig. 4 (a) Profile of the frictional pressure loss along the production well MT-4. (b, c) Profiles of the friction factor and roughness determined from the frictional pressure loss. The roughness determined using Eq. (6) is only valid below the flash point.

Fig. 5 Assumed casing hydraulic diameter for decomposing the measured pressure at the testing well K-1 along with the schematic casing program.

Fig. 6 (a) Results of the pressure–temperature logging for the first and second runs (Runs 1 and 2) at the testing well K-1. (b, c) Decomposition of the measured pressure into components for each run. The frictional component is shown on the upper (↑) and lower (↓) scales. The multistage cementing tool is referred to as MCT.

Fig. 7 (a) Profile of the frictional pressure loss along the testing well K-1 below the flash point. (b, c) Profiles of the friction factor and roughness determined from the frictional pressure loss. The multistage cementing tool is referred to as MCT.

Fig. 8 Profiles of the frictional pressure loss along the testing well K-1 below the flash point, compared with the inclination (a) and cable tension (b). The multistage cementing tool denoted by the squares is referred to as MCT. The circles denote the end of the buildup section of inclination.

Matsumoto et al., Fig. 1

Original size: 6.0 cm × 7.0 cm

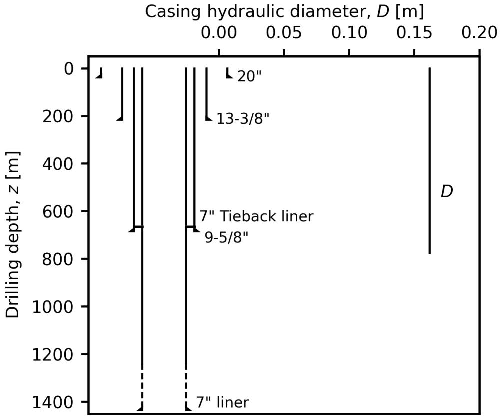

Matsumoto et al., Fig. 2

Original size: 8.0 cm × 7.0 cm

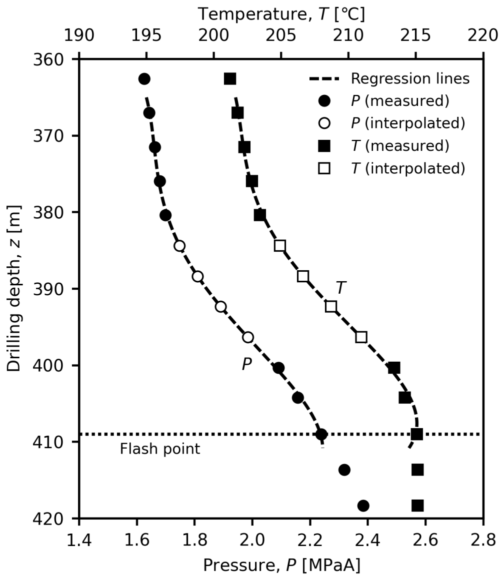

Matsumoto et al., Fig. 3

Original size: 9.0 cm × 14.0 cm

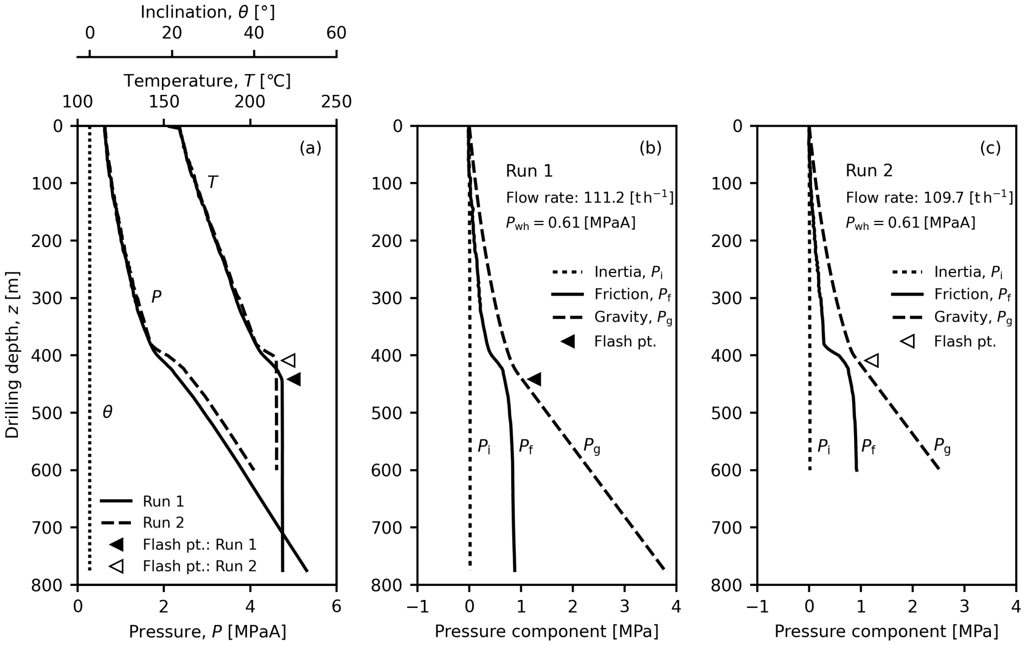

Matsumoto et al., Fig. 4

Original size: 8.0 cm × 14.0 cm

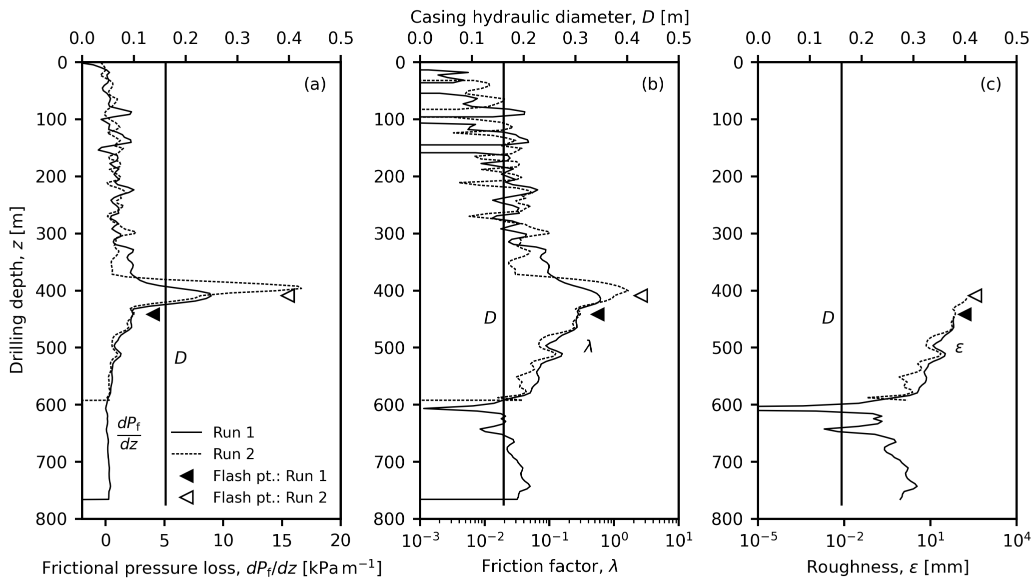

Matsumoto et al., Fig. 5

Original size: 6.0 cm × 7.0 cm

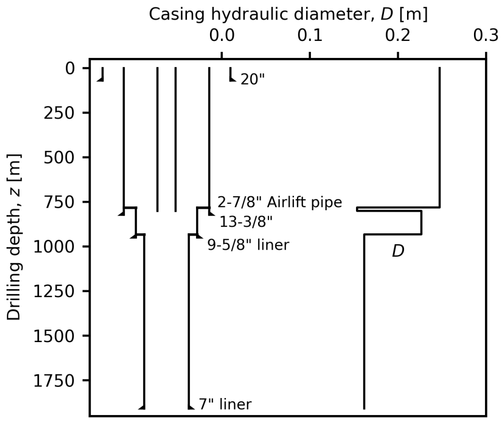

Matsumoto et al., Fig. 6

Original size: 9.0 cm × 14.0 cm

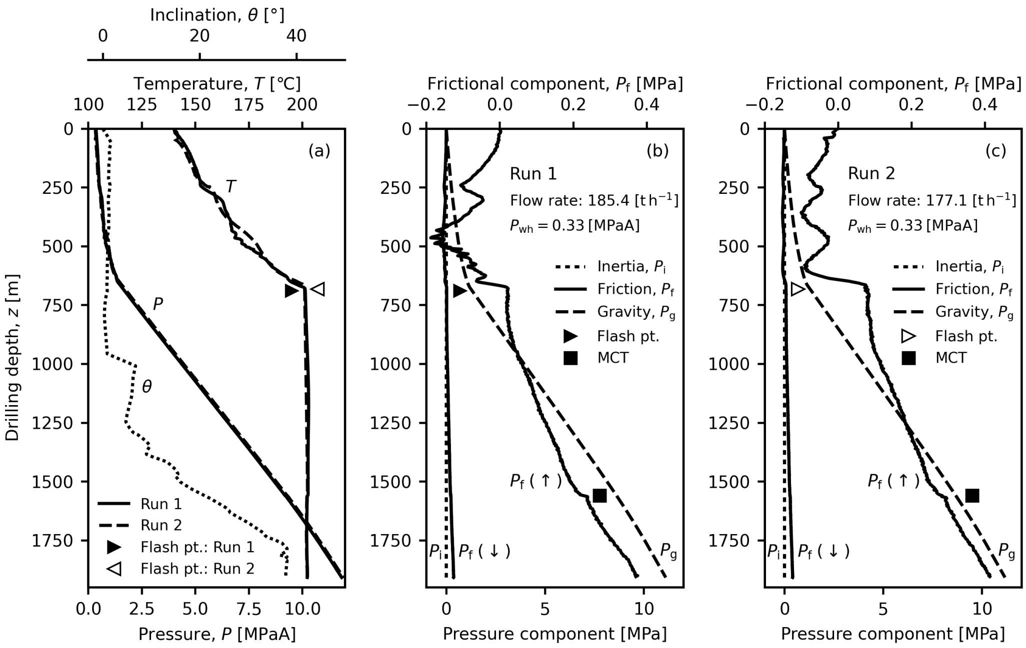

Matsumoto et al., Fig. 7

Original size: 8.0 cm × 14.0 cm

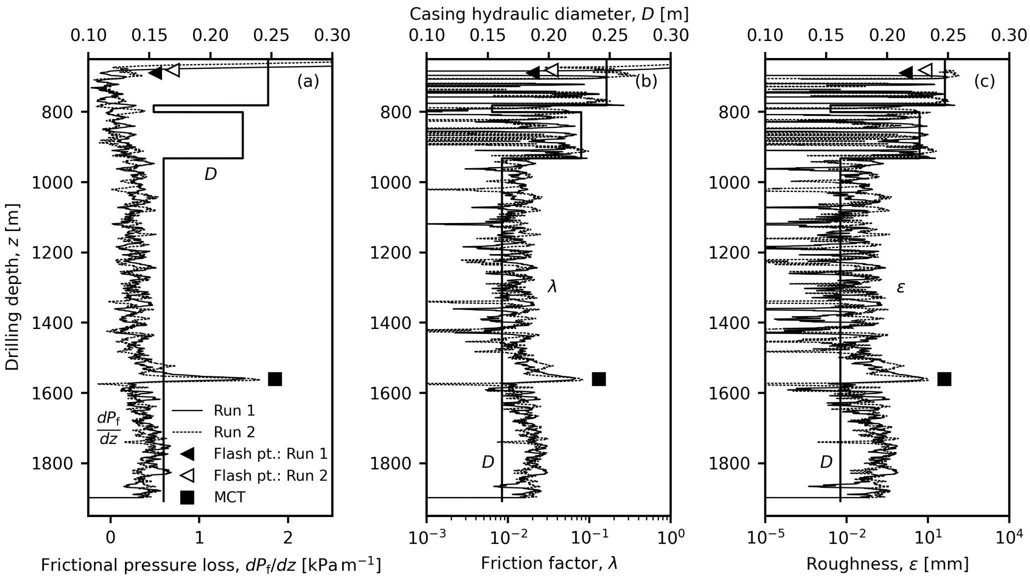

Matsumoto et al., Fig. 8

Original size: 8.0 cm × 10.0 cm